Stress Distribution in the Western India-Eurasia Collision Zone: A Region of Varying Stress Fields in a Compressional Regime

R. Arun Prasath*, Brijesh K. Bansal, Mithila Verma

Ministry of Earth Sciences, Seismology Division, Prithvi Bhavan, Lodhi Road, New Delhi, India.

*devanthran@hotmail.com | arun.devanthran@nic.in

Keywords:

India-Eurasia Collision Zone; Stress Distribution; Garhwal-Kumaun Himalaya; Kashmir Earthquake; Karakorum Fault; Kaurik Chango Rift

Abstract

The western India-Eurasia collision zone (IECZ) has experienced devastating earthquakes in the past century and continues to be seismically active. However, the Stress regime and Seismotectonics of the region remains poorly understood. In view of this, we carried out iterative, joint stress inversions of 245 well-constrained earthquake focal mechanisms to constrain the stress regime and its spatial variability in the region and dwell upon their implications for earthquake generation. Salient new findings from the study are, (i) the Kangra-Chamba-Kishtwar region shows arc-oblique horizontal maximum compressive stress (σ1, WSW-ENE) in contrast to arc-normal (NNE-SSW) in other regions of the Himalaya, (ii) the Kashmir earthquake sequence (in 2005) and its epicentral region i.e. the Hazara Syntaxis show similar stress patterns with that of the Central Himalaya, (iii) Nanga Parbat Syntaxis experiences pure extension, and (iv) Kaurik Chango Rift, with N-S trending σ1, probably extends deep into the Karakoram fault. Based on these findings, we categorize the region into six state of stress fields consistent with geology and plate motion models. The magnitudes for these stress fields show a decreasing trend from 0.90 in the southeast (Garhwal-Kumaun-Shimla) to 0.46 in the northwest (Hazara Syntaxis) and 0.39 in the northeast (Karakoram) suggesting multiple tectonic forces in northwestern and northeastern regions. The study reveals heterogeneity in the stress field within the western IECZ, induced by tectonic forces and structural variability.

1. Introduction

India-Eurasia Collision Zone (IECZ), predominantly compressional in nature, was formed by a continent-continent collision during the Eocene period, not more than 57 Ma ago

(Molnar & Tapponnier, 1977; Leech et al., 2005). The region has a diverse tectonic setting spanning the great Himalayan intra-crustal thrusts to the normal faults in the Tethyan-Tibetan regions and numerous transverse structures of the region (Molnar & Tapponnier, 1977; Tapponnier et al., 1981). The IECZ has experienced a number of destructive earthquakes such as, M_w 8.2 Bihar-Nepal earthquake (1934), M_w 7.6 Kashmir earthquake (2005) and M_w 7.8 Nepal earthquake (2015) owing to the continuing plate convergence of 37-44 mm/yr (Arora et al., 2017; Avouac et al, 2006; Banerjee & Bürgmann, 2002; Sapkota et al., 2013). In the western IECZ, the majority of the earthquakes occur along a linear trend known as Himalayan Seismic Belt (HSB). The HSB is positioned around two intra-crustal boundary thrusts, viz., the Main Central Thrust and the Main Boundary Thrust. Besides, two major structures in the Tibetan Plateau, viz., the Karakoram Fault, a dextral fault and the Kaurik Chango Rift (KCR), a transverse and trans-tensional structure located between Karakoram Fault and the Himalayan wedge are also experiencing moderate earthquake activity (Gahalaut & Kundu, 2012; Ni & Barazangi, 1984).

Imaging the crustal stress field using double-couple earthquake focal mechanisms (FM) could provide crucial information to understand the tectonic stress regime, its variation and the role of local and transverse tectonics that are responsible for earthquake generation and help constrain the kinematics, earthquake nucleation processes and hazard estimation. A few earlier studies have attempted to image the stress field of the region utilizing the available FM solutions in small patches (Gahalaut & Rao, 2009; Mahesh et al., 2015; Prasath et al., 2017; Yadav et al., 2016; Yadav et al., 2017). However, some of these studies were based on the FM solutions of micro-earthquakes of magnitudes $1.5<M<3.0$ with low azimuthal coverage and less polarity readings. Recent advancements in the seismic networks of this

region and advanced inversion techniques developed in the 21st century have helped in achieving more stable and reliable moment tensor solutions as small as M_w 3.0 (D'Amico, 2018; see also Prasath et al., 2017). In the present study, we utilize a catalog of 245 reliable FM solutions for earthquakes with magnitudes of 3.0≤M≤7.6 to image the current stress field, its variability and to understand the dominant forces and Seismotectonics of the western IECZ (Figures 1 and 2; Supplementary Tables S1-S3).

2. Structural Framework

The structural framework of the study area is highly complex, which comprises of the western Himalayan Syntaxial zone, Western Himalaya, Garhwal-Kumaun sector of the Central Himalaya and the western Tibetan region. The Himalayan wedge (western and central Himalaya), which is sandwiched between the southern Tibet in the north and the Indo Gangetic plains in the south, comprises of major intra-crustal boundary faults viz., (i) the Himalayan Frontal Thrust (HFT), (ii) Main Boundary Thrust (MBT), (iii) Main Central Thrust (MCT), (iv) Southern Tibetan Detachment (STD) and (v) Indus Tsangpo Suture (ITS) (Figure 1) (Gansser, 1964). These northward dipping structures are dividing the region into different litho-tectonic zones viz., (from south to north), Sub Himalaya (SH), Lesser Himalaya (LH), Higher Himalayan Crystallines (HHC) and Tethyan Himalaya (TH) (Figure 1) (Gansser, 1964). Other significant structural features in the Himalayan wedge are the Kishtwar Window (KW), the Kullu-Larji-Rampur Window (KLRW) and the Almora Klippen (AK) (Figure 1).

The Western Himalayan Syntaxial zone comprising of (i) Salt Range Thrust (SRT, an equivalent to the HFT), (ii) Main Mantle Thrust (MMT, *aka* Shyok Suture zone, which is an

92 equivalent to the ITS) and (iii) Main Karakorum Thrust (MKT). This zone also includes
93 Nanga Parbat Syntaxis in its northwest and Hazara Syntaxis in its core, where the M_w 7.6
94 Kashmir earthquake of 2005 had occurred. The other significant geological features in this
95 part of the region are (i) Balakot Bagh Fault (BBF) and (ii) Jhelum Fault (JF) and (iii) the
96 Srinagar Basin (SB), in which the Srinagar basin demonstrate very less seismicity in
97 comparison to the adjacent regions (Figure 1).

98 The major faults of the Himalayan wedge are sole to a shallow and north dipping basal
99 detachment aka the Main Himalayan Thrust (MHT) located between the depths of 10 and 20
100 km beneath the region (Ni & Barazangi, 1984). The MHT is locked along the plate interface
101 with 100-120 km coupling width, however the Syntaxial zone have the broader width of 140-
102 180 km (Li et al., 2018 and references there in).

103 The northeastern part of the study region i.e. the western Tibet is occupied by the
104 Karakoram Fault (KF), a dextral fault of ~800 km long, dividing the Tibetan plateau into two
105 parts (Leech, 2008; Phillips et al., 2004). This region also comprises of two major sinistral
106 faults viz., Longmu Gozha Fault (LGF, an equivalent to the MKT), and Karakax Fault (KXF)
107 (Figure 1). The convergence rate along the Leh-Ladakh region is 17.8±1 mm/yr., while the
108 Western Himalaya and the Garhwal-Kumaun sector of the Central Himalaya are having less
109 convergence, at the rate of ~15 mm/yr. (Banerjee et al., 2008; Banerjee & Bürgmann, 2002;
110 Jade et al., 2014, 2017; Mondal et al., 2016 and references there in). South of the KF, lies the
111 Kaurik Chango Rift (KCR), a transverse structure, which is suggested to have a seismogenic
112 relationship to the earthquakes of the Garhwal Himalaya located south of this rift (Arora et
113 al., 2012). The KCR have also been linked to an inherited basement structure that exists

beneath the Garhwal Himalaya i.e. the Delhi-Haridwar Ridge (DHR), trending NE-SW, almost perpendicular to the major Himalayan structures.

3. Data and Methodology

The FM data have been compiled from 25 different sources comprising of various literature that also includes the solutions from Global Centroid Moment Tensor (GCMT) catalog (Baranowski et al., 1984; Chandra et al., 1974; Das Gupta et al., 1982; Dziewonski et al., 1981; Ekström et al., 2012; Gahalaut & Rao, 2009; Hazarika et al., 2017; Kanna et al., 2018; Mahesh et al., 2015; Negi et al., 2017; Parija et al., 2018; Paul et al., 2018; Prasath et al., 2017; Ram et al., 2005; Rastogi, 1974; Singh et al., 2018; Srinagesh et al., 2018; Kumar et al., 2009; Molnar & Chen, 1983; Molnar & Lyon-Caent, 1989; Srivastava et al., 1987; Tandon & Srivastava, 1975; Verma and Sekhar, 1986; Verma et al., 2015; Yadav et al., 2016) (Supplementary Tables S1-S3). Initially, more than 320 solutions were considered, however only 245 FM solutions which passed our quality criteria have been chosen. The primary criterion was to select crustal earthquakes with magnitude M≥3.0. Majority of those (N=210) are located in the upper crust in the 0-25 km depth range with maximum depth being 66 km. Due weightage was given to quality of the solutions, viz., (i) the technique used, (ii) the availability of local network data, and (iii) well constrained results with minimal errors. In the instance of multiple solutions with moment tensors against other type of FM solutions such as FOCMEC and INVRAD, the moment tensor solutions were preferred due to their reliability and better constraints. Also, in case of multiple solutions with similar techniques, only those obtained using local networks and with larger number of station records were chosen; e.g., in the case of the M_L 5.5 Dharamshala earthquake (1986) which has multiple solutions, the one

that utilized the local network data and has better azimuthal coverage was chosen (Ram et al., 2005). In the resultant catalog of 245 solutions, 186 are from the moment tensor inversion techniques, while the remaining are from a combination of one or more of the following, (i) Body-wave synthetic matching, (ii) P-wave first motion polarity readings and (iii) Amplitude inversions.

We used an iterative joint inversion technique to obtain stress and fault orientations, which is based on the inversion method of Michael (1987). The inversion was performed in MATLAB environment using the program STRESSINVERSE (Vavryčuk, 2014). It produces three principle stress directions (σ1- σ3) and stress magnitude *aka* shape ratio 'R' (R-value) using the following relation (Gephart & Forsyth, 1984).

$$R = {(\sigma 1 - \sigma 2)}/{(\sigma 1 - \sigma 3)} \quad \text{- (1)}$$

The program makes use of both the nodal planes of each FM solutions and identifies the faults using an instability analysis. The instability analysis was performed with the nominal values of 0 to 1 and the maximum value being the maximum possibility for being ruptured. While carrying out the instability analysis, the friction coefficient (FC) 'μ' is estimated. The identified faults were plotted on a Mohr circle diagram to identify the optimal planes.

To address the local variations in stress field, we have divided the region into nine seismotectonic zones based on its geology, tectonics, faulting type and geographical proximity of the FM solutions, viz., Garhwal-Kumaun Himalaya (GKH), Shimla Hills, Kangra-Chamba, Kishtwar, epicentral region of the Kashmir earthquake (Hazara Syntaxis), Nanga Parbat Syntaxis, Northwest KF, Southeast KF and KCR (Figure 2). Besides, the

inversion has also been performed separately for the aftershocks of the 2005 Kashmir earthquake to understand its stress pattern.

Since the available FM solutions show a spatial variability, we further categorized the data into two sets, viz., (i) HSB with thrust-type solutions, and (ii) north of HSB with strike-slip and normal fault type solutions. Further, we performed an inversion for the complete dataset (Table 1). For each inversion, we compute the best-fitting stress field vectors, viz., compressive (σ1), intermediate (σ2) and tensile (σ3), the shape ratio *aka* the stress magnitude (R-value), Coefficient of Friction (FC) and Optimally Oriented Fault planes (hereafter referred to as optimal planes), which governs the susceptibility of a fault to be ruptured under the given stress conditions.

4. Results and Discussion

The overall stress inversion for the western IECZ shows a compressional tectonic regime with dominant σ1 oriented towards NE-SW and R-value of 0.7 (Figure 3, Table 1, and Supplementary Figure S1). However, the zone-wise results obtained show varying tectonic stress regimes and orientations for different zones suggesting significant heterogeneity in the stress field of the region. These are explained below.

4.1 Compressional stress regime

The GKH and Shimla regions show compressional stress regime with sub-horizontal and arc-normal σ1 (NE-SW), in good agreement with the direction of relative motion of Indian plate (Figure 3). The high R-value of 0.93 and 0.85 for GKH and Shimla, respectively show that the generation of seismogenic stress in these regions is controlled predominantly by

σ1 (Table 1). The plunge of σ1 for both the regions are found to be 19º, consistent with the preferred nodal planes of optimal planes (25º and 26º, respectively), which suggests active deformation along the mid-crustal ramp of the detachment having a shallow dip of <25º (Ni & Barazangi, 1984). Besides, the low FC obtained for both the regions (0.66 and 0.7 for GKH and Shimla, respectively) along with low b-value and the occurrence of low-velocity zones reported in the literature suggest the presence of fluids and their role in earthquake generation processes (Mahajan et al., 2010; Prasath et al., 2017; Rawat et al, 2014).

Despite having similar (compressional) stress regimes, the Kangra-Chamba and Kishtwar regions show arc-oblique principle compressive stress (σ1≠90º to the Himalayan Arc, ~65º in this context) in comparison to the arc-normal principle compressive stress (σ1=90º to the Arc) for GKH and Shimla regions (Figure 3). Further, the moderate R-value (0.62 and 0.78, respectively) and relatively high FC (0.85 and 1.2) estimated for these regions are different than the GKH and Shimla regions (Table 1). Previous studies based on the erosional rates, thermo-chronology, topography, geomorphogical indicators and earthquake moment tensors have proposed the 77º N longitude, which separates GKH and Shimla Hills zones from Kangra-Chamba and Kishtwar zones, as a transition between contradictory tectonic settings on either side (Eugster et al., 2018; Nennewitz et al., 2018). Also, Seeber & Pêcher (1998) proposed that the India-Eurasia convergence is arc-normal in the central Himalaya and becomes arc-oblique in the western Himalaya, which is consistent with the recent plate motion models by Kundu et al. (2014), where slip vectors mark the arc-normal convergence in Central Himalaya (including GKH and Shimla zones) and oblique convergence in Western Himalaya (Kangra-Chamba, Kishtwar and Kashmir zones). The oblique convergence along western Himalaya produces pure-shear along the KF, located

204 northeast of this region and thrusting along the Himalayan intra-crustal thrusts. This is well
205 correlated with the arc-oblique stress orientations for Kangra-Chamba and Kishtwar zones in
206 the present study. Apparently, the change in convergence perturbs the regional stress field and
207 produces the arc-oblique stress field in the region.

208 The inversion of FM solutions in the epicentral region of 2005 Kashmir earthquake
209 (Hazara Syntaxis) and separately for its aftershocks shows little difference, suggestive of
210 similar stress orientations before, during and after the Kashmir earthquake (Figure 3,
211 Supplementary Figure S1). The stress orientations for the surrounding regions are not
212 compatible with this region, viz., WSW-ENE oriented compressional regime in the Kangra-
213 Chamba and Kishtwar regions and NNE-SSW oriented compressional regime in Hindu Kush
214 and NE-SW oriented strike-slip tectonics in Pamir region (Gahalaut & Rao, 2009). In an
215 earlier study, the stress orientations of the Kashmir earthquake and Hazara Syntaxis were
216 compared with that of the Himalaya, leading to apprehension over its origin being a
217 Himalayan earthquake (Gahalaut & Rao, 2009). However, those studies used earthquake FM
218 solutions for the entire Himalayan Arc that includes the earthquakes from Central and Eastern
219 Himalaya as well. In the present study, the stress orientations for the Kashmir earthquake
220 sequence and Hazara Syntaxis are found to be similar to that of the Central Himalaya (GKH
221 and Shimla zones), which strongly suggests that the Kashmir earthquake to be a Himalayan
222 earthquake. The optimal planes for the Hazara Syntaxis and for the aftershock sequence
223 (N=84) of Kashmir earthquake show shallow dip angles (21° and 22°, respectively), similar to
224 the mid-crustal ramp of the Central Himalaya (≤25°) (Table 1) (Gahalaut & Kalpna, 2001;
225 Prasath et al., 2017, 2019; Seeber et al., 1981). Further, the low R-value (0.4) for Hazara
226 Syntaxis and moderate value (0.6) for the aftershock sequence reveal a major role of σ1

during the aftershock activity and also suggest an interplay of the varying tectonic settings on earthquake generation mechanisms in the region (Hindu Kush, Pamir and the Himalaya). The low FC values (0.4-0.45) suggest that the faults in this region are weak and support the presence of fluids, which is generally believed to affect the large earthquake generation processes and control the aftershock genesis (Yu et al., 2019).

4.2. Strike-slip and extensional stress regimes

The stress fields in HSB and Western Tibet regions show distinctive stress regimes with compressional and strike-slip tectonics, respectively with varying R-values (0.91 and 0.4, respectively), suggesting predominant role of plate motion driven tectonic forces in HSB and multiple tectonic forces in Western Tibet (Table 1). The optimal planes suggest that the faults are steeper in Tibetan region with near-vertical dip angles in contrast to the faults with shallow dip angle in HSB. The friction on the faults along HSB as well as Tibetan region have been estimated to be ~0.7 and 0.64, which suggest the role of fluids in earthquake generation and nucleation in IECZ (Table 1) (Prasath et al., 2017, 2019; Rawat et al., 2014; Kumar et al., 2013, 2019).

The seismicity in the regions around KF is concentrated in the northwestern zone but diffuse in the southeastern zone. We perform inversions separately for these two zones in order to understand the stress distribution along this fault. The northwestern zone show strike-slip tectonics with NE-SW oriented σ1 similar to that of the Himalayan regions and suggests active nature of KF. However, the southeastern zone shows strike-slip tectonics with nearly N-S oriented sub-horizontal σ1. Similarly, the R-value found to be varying from 0.39 in northwest to 0.65 in southeast, consistent with the slip rates estimated for northwestern (5 mm/yr.) and southeastern (3.6 mm/yr.) parts of KF (Kundu et al., 2014). The data therefore

suggests the complex nature of stress field along KF, owing potentially to the association of local and regional faults, viz., KCR, Karakax fault, Main Karakoram thrust and Longmu Gozha fault. The FC values for northwestern and southeastern zones (0.71 and 0.82, respectively) are close to the values estimated for Himalayan regions such as Kishtwar and GKH (Table 1). The stress orientations along KCR show that the region is currently experiencing oblique-slip tectonics with near-vertical σ2 and N-S oriented, sub-horizontal σ1, which is compatible with that of geological, seismological and plate motion models, suggesting that the KCR region is experiencing E-W directed trans-tension (DiPietro et al., 2000; Dziewonski et al., 1981; Gahalaut and Kundu., 2012; Jade et al., 2014; Tapponnier et al., 1981). Moreover, the moderate R-value (0.53) suggests involvement of multiple tectonic forces in generation of earthquakes around this rift. The southeast KF and KCR zones are found to be consistent as the inversion yields almost similar results and supports the previous claims that the KCR may be extending deep into KF and segmenting it[25]. Hence, we categorize these two zones as a single stress field. The Nanga Parbat Syntaxis, which is located between the Kohistan Arc and Ladakh Arc show predominantly extensional tectonics, ruling out any role of the Main Mantle Thrust (MMT) in generation of seismicity in this region. Moreover, the optimal planes suggest the causative fault to be normal with steep dip (~60º), further suggesting that the stress regime is controlled by the normal faulting along the Kohistan Arc (DiPietro et al., 2000; Seeber & Pêcher, 1998). The moderate R-value (0.63) suggests the reasonable involvement of multiple tectonic stresses (Table 1) similar to the Hazara Syntaxis.

4.3. State of stress fields

Based on the detailed analysis of stress orientations, we classify the western IECZ into six state of stress fields consistent with geomorphology, geology and plate motion models (Figure 3). These are, (I) GKH-Shimla (ID 14), (II) Kangra-Chamba-Kishtwar (ID 15), (III) Hazara Syntaxis (ID 5), (IV) Nanga Parbat Syntaxis (ID 7), (V) northwest KF (ID 8) and (VI) southeast KF-KCR (ID 16) (Figures 3 and 4 and Supplementary Figure S1). Despite their different tectonic setup, the stress fields I and III share similar properties with compressional regime and arc-normal horizontal compressive stresses. However, their stress magnitudes differ substantially (0.9 and 0.42 for GHK-Shimla and Hazara Syntaxis, respectively) owing to their structural and tectonic association, where the Hazara Syntaxis located in the terminal end of the Himalaya surrounded by Hindu Kush and Pamir regions in contrast to the GHK-Shimla regions that are located entirely within the Himalaya. In contrast to these stress fields, the stress field II shows compressional regime with arc-oblique horizontal stress field. The stress field IV, i.e. Nanga Parbat Syntaxis shows predominantly extensional regime. While the stress fields V and VI show strike-slip tectonic regime, the relative plate motion is the dominant force in these regions too. The spatial distribution of stress fields shows a decreasing trend in stress magnitude (R-value) from southeast (0.90 in GKH-Shimla) to Kangra-Chamba-Kishtwar (0.72) and northwest (0.46 in Hazara Syntaxis). A similar trend has been observed in the northeast with 0.52 for southeast KF-KCR and 0.39 for northeast KF. The low stress magnitudes coincide with the regions having multiple tectonic forces involving Hindu Kush, Pamir and the Himalaya in the northwestern end of the region (Hazara Syntaxis) and local and regional faults, viz., KF, KXF and LGF in the northeastern part (Karakoram Ranges).

5. Conclusion

Our study confirms that the western IECZ is characterized by a heterogeneous stress field. This heterogeneity exists mainly because of the variation in the India-Eurasia convergence, local and regional structures, multiple tectonic forces and the presence of fluids in the region. Zone-wise analysis of focal mechanism solutions provide the following new insights: (i) Arc-normal compression in Garhwal-Kumaun-Shimla region and arc-oblique compression in Kangra-Chamba-Kishtwar region, (ii) Himalayan-type stress orientations for Kashmir earthquake (2005) and Hazara Syntaxis, (iii) Pure extension at Nanga Parbat Syntaxis, and (iv) Extension of the transverse feature KCR, with N-S trending $\sigma 1$, deep into KF. From these inferences, we categorize the region into six state of stress fields. The decreasing trend in stress magnitudes from the southeast to the northwest suggests the presence of multiple tectonic forces towards northwestern (Hazara Syntaxis) and northeastern (Karakoram) regions. The new results will be useful for simulation of geodynamic stress field, earthquake nucleation processes and seismic hazard assessments.

Acknowledgments

The study is supported by Ministry of Earth Sciences, Govt. of India. We acknowledge Dr. Vineet Gahalaut for suggestions and Prof. Vaclav Vavryčuk for providing valuable comments on the work. Suggestions made by Dr. S. Roy significantly improved the manuscript. We also thank Komal, Joyeeta, Ojaswita, Mayank, Medha and Dhamu for their help and support. The data used in this study are compiled from different sources viz., ISC Catalog, Global CMT

catalog, published journal articles and it can be accessed collectively from the supplementary tables or their respective sources, as mentioned in the article.

Competing Interests

The authors declare no competing interests.

References

1. Arora, B. R., Bansal, B. K., Prajapati, S. K., Sutar, A. K., & Nayak, S. (2017). Seismotectonics and seismogenesis of Mw7. 8 Gorkha earthquake and its aftershocks. *Journal of Asian Earth Sciences*, *133*, 2-11.
2. Arora, B. R., Gahalaut, V. K., & Kumar, N. (2012). Structural control on along-strike variation in the seismicity of the northwest Himalaya. *Journal of Asian Earth Sciences*, *57*, 15-24.
3. Avouac, J. P., Ayoub, F., Leprince, S., Konca, O., & Helmberger, D. V. (2006). The 2005, Mw 7.6 Kashmir earthquake: Sub-pixel correlation of ASTER images and seismic waveforms analysis. *Earth and Planetary Science Letters*, *249*(3-4), 514-528.
4. Banerjee, P., & Bürgmann, R. (2002). Convergence across the northwest Himalaya from GPS measurements. *Geophysical Research Letters*, *29*(13), 30-1.
5. Banerjee, P., Bürgmann, R., Nagarajan, B., & Apel, E. (2008). Intraplate deformation of the Indian subcontinent. *Geophysical Research Letters*, *35*(18).

6. Baranowski, J., Armbruster, J., Seeber, L., & Molnar, P. (1984). Focal depths and fault plane solutions of earthquakes and active tectonics of the Himalaya. *Journal of Geophysical Research: Solid Earth*, *89*(B8), 6918-6928.
7. Chandra, U. (1978). Seismicity, earthquake mechanisms and tectonics along the Himalayan mountain range and vicinity. *Physics of the Earth and Planetary Interiors*, *16*(2), 109-131.
8. Chaudhury, H. M., Srivastava, H. N., & Rao, J. S. (1974). Seismotectonic investigations of the Himalayas. *Him. Geol*, *4*, 481-491.
9. D'Amico, S. (Ed.). (2018). *Moment Tensor Solutions: A Useful Tool for Seismotectonics*. Springer.
10. Das Gupta, A., Srivastava, H. N., & Basu, M. S. (1982). Source mechanism of earthquakes in Kangra–Chamba region of Himachal Pradesh, India. *Bull. Ind. Soc. Earthq. Tech*, *19*, 102-116.
11. DiPietro, J. A., Hussain, A., Ahmad, I., & Khan, M. A. (2000). The Main Mantle Thrust in Pakistan: its character and extent. *Geological Society, London, Special Publications*, *170*(1), 375-393.
12. Dziewonski, A. M., Chou, T. A., & Woodhouse, J. H. (1981). Determination of earthquake source parameters from waveform data for studies of global and regional seismicity. *Journal of Geophysical Research: Solid Earth*, *86*(B4), 2825-2852.
13. Ekström, G., Nettles, M., & Dziewoński, A. M. (2012). The global CMT project 2004–2010: Centroid-moment tensors for 13,017 earthquakes. *Physics of the Earth and Planetary Interiors*, *200*, 1-9.

14. Eugster, P., Thiede, R. C., Scherler, D., Stübner, K., Sobel, E. R., & Strecker, M. R. (2018). Segmentation of the Main Himalayan Thrust Revealed by Low-Temperature Thermochronometry in the Western Indian Himalaya. *Tectonics*, *37*(8), 2710-2726.
15. Gahalaut, K. and Rao, N.P., 2009. Stress field in the western Himalaya with special reference to the 8 October 2005 Muzaffarabad earthquake. *Journal of seismology*, *13*(3), p.371.
16. Gahalaut, V. K., & Kalpna. (2001). Himalayan mid-crustal ramp. *Current Science*, 1641-1646.
17. Gahalaut, V. K., & Kundu, B. (2012). Possible influence of subducting ridges on the Himalayan arc and on the ruptures of great and major Himalayan earthquakes. *Gondwana Research*, *21*(4), 1080-1088.
18. Gephart, J. W., & Forsyth, D. W. (1984). An improved method for determining the regional stress tensor using earthquake focal mechanism data: application to the San Fernando earthquake sequence. *Journal of Geophysical Research: Solid Earth*, *89*(B11), 9305-9320.
19. Gansser, A. (1964). Geology of the Himalayas: London, Wiley Interscience, 289 pp.
20. Hazarika, D., Paul, A., Wadhawan, M., Kumar, N., Sen, K., & Pant, C. C. (2017). Seismotectonics of the Trans-Himalaya, Eastern Ladakh, India: Constraints from moment tensor solutions of local earthquake data. *Tectonophysics*, *698*, 38-46.
21. Hintersberger, E., Thiede, R. C., Strecker, M. R., & Hacker, B. R. (2010). East-west extension in the NW Indian Himalaya. *Bulletin*, *122*(9-10), 1499-1515.
22. ISC (2019). International Seismological Centre, online bulletin, http://www.isc.ac.uk , Thatcham, United Kingdom.

23. Jade, S., Mukul, M., Gaur, V. K., Kumar, K., Shrungeshwar, T. S., Satyal, G. S., ... & Banerjee, S. (2014). Contemporary deformation in the Kashmir–Himachal, Garhwal and Kumaon Himalaya: significant insights from 1995–2008 GPS time series. *Journal of Geodesy*, *88*(6), 539-557.

24. Jade, S., Shrungeshwara, T. S., Kumar, K., Choudhury, P., Dumka, R. K., & Bhu, H. (2017). India plate angular velocity and contemporary deformation rates from continuous GPS measurements from 1996 to 2015. *Scientific reports*, *7*(1), 1-16.

25. Kanna, N., Gupta, S., & Prakasam, K. S. (2018). Micro-seismicity and seismotectonic study in Western Himalaya–Ladakh-Karakoram using local broadband seismic data. *Tectonophysics*, *726*, 100-109.

26. Kumar, N., Aoudia, A., Guidarelli, M., Babu, V. G., Hazarika, D., & Yadav, D. K. (2019). Delineation of lithosphere structure and characterization of the Moho geometry under the Himalaya–Karakoram–Tibet collision zone using surface-wave tomography. *Geological Society, London, Special Publications*, *481*(1), 19-40.

27. Kumar, N., Arora, B. R., Mukhopadhyay, S., & Yadav, D. K. (2013). Seismogenesis of clustered seismicity beneath the Kangra–Chamba sector of northwest Himalaya: constraints from 3D local earthquake tomography. *Journal of Asian Earth Sciences*, *62*, 638-646.

28. Kumar, N., Sharma, J., Arora, B. R., & Mukhopadhyay, S. (2009). Seismotectonic model of the Kangra–Chamba sector of northwest Himalaya: Constraints from joint hypocenter determination and focal mechanism. *Bulletin of the Seismological Society of America*, *99*(1), 95-109.

29. Kundu, B., Yadav, R. K., Bali, B. S., Chowdhury, S., & Gahalaut, V. K. (2014). Oblique convergence and slip partitioning in the NW Himalaya: Implications from GPS measurements. *Tectonics*, *33*(10), 2013-2024.
30. Leech, M. L. (2008). Does the Karakoram fault interrupt mid-crustal channel flow in the western Himalaya?. *Earth and Planetary Science Letters*, *276*(3-4), 314-322.
31. Leech, M. L., Singh, S., Jain, A. K., Klemperer, S. L., & Manickavasagam, R. M. (2005). The onset of India–Asia continental collision: early, steep subduction required by the timing of UHP metamorphism in the western Himalaya. *Earth and Planetary Science Letters*, *234*(1-2), 83-97.
32. Li, S., Wang, Q., Yang, S., Qiao, X., Nie, Z., Zou, R., ... & Chen, G. (2018). Geodetic imaging mega-thrust coupling beneath the Himalaya. *Tectonophysics*, *747*, 225-238.
33. Mahajan, A. K., Thakur, V. C., Sharma, M. L., & Chauhan, M. (2010). Probabilistic seismic hazard map of NW Himalaya and its adjoining area, India. *Natural Hazards*, *53*(3), 443-457.
34. Mahesh, P., Gupta, S., Saikia, U. and Rai, S.S., 2015. Seismotectonics and crustal stress field in the Kumaon–Garhwal Himalaya. *Tectonophysics*, *655*, pp.124-138.
35. Michael, A. J. (1987). Use of focal mechanisms to determine stress: a control study. *Journal of Geophysical Research: Solid Earth*, *92*(B1), 357-368.
36. Molnar, P., & Chen, W. P. (1983). Focal depths and fault plane solutions of earthquakes under the Tibetan plateau. *Journal of Geophysical Research: Solid Earth*, *88*(B2), 1180-1196.

37. Molnar, P., & Lyon-Caent, H. (1989). Fault plane solutions of earthquakes and active tectonics of the Tibetan Plateau and its margins. *Geophysical Journal International*, *99*(1), 123-153.
38. Molnar, P., & Lyon-Caent, H. (1989). Fault plane solutions of earthquakes and active tectonics of the Tibetan Plateau and its margins. *Geophysical Journal International*, *99*(1), 123-153.
39. Molnar, P., & Tapponnier, P. (1977). The collision between India and Eurasia. *Scientific American*, *236*(4), 30-41.
40. Mondal, S. K., Borghi, A., Roy, P. N. S., & Aoudia, A. (2016). GPS, scaling exponent and past seismicity for seismic hazard assessment in Garhwal–Kumaun, Himalayan region. *Natural Hazards*, *80*(2), 1349-1367.
41. Negi, S. S., Paul, A., Cesca, S., Kriegerowski, M., Mahesh, P., & Gupta, S. (2017). Crustal velocity structure and earthquake processes of Garhwal-Kumaun Himalaya: Constraints from regional waveform inversion and array beam modeling. *Tectonophysics*, *712*, 45-63.
42. Nennewitz, M., Thiede, R. C., & Bookhagen, B. (2018). Fault activity, tectonic segmentation, and deformation pattern of the western Himalaya on Ma timescales inferred from landscape morphology. *Lithosphere*, *10*(5), 632-640.
43. Ni, J., & Barazangi, M. (1984). Seismotectonics of the Himalayan collision zone: Geometry of the underthrusting Indian plate beneath the Himalaya. *Journal of Geophysical Research: Solid Earth*, *89*(B2), 1147-1163.

44. Parija, M. P., Kumar, S., Tiwari, V. M., Rao, N. P., Kumar, N., Biswal, S., & Singh, I. (2018). Microseismicity, tectonics and seismic potential in the Western Himalayan segment, NW Himalaya, India. *Journal of Asian Earth Sciences*, *159*, 1-16.

45. Paul, H., Priestley, K., Powali, D., Sharma, S., Mitra, S., & Wanchoo, S. (2018). Signatures of the existence of frontal and lateral ramp structures near the Kishtwar Window of the Jammu and Kashmir Himalaya: evidence from microseismicity and source mechanisms. *Geochemistry, Geophysics, Geosystems*, *19*(9), 3097-3114.

46. Paul, J., Bürgmann, R., Gaur, V. K., Bilham, R., Larson, K. M., Ananda, M. B., ... & Kumar, D. (2001). The motion and active deformation of India. *Geophysical Research Letters*, *28*(4), 647-650.

47. Phillips, R. J., Parrish, R. R., & Searle, M. P. (2004). Age constraints on ductile deformation and long-term slip rates along the Karakoram fault zone, Ladakh. *Earth and Planetary Science Letters*, *226*(3-4), 305-319.

48. Prasath, R. A., Paul, A., & Singh, S. (2017). Upper crustal stress and seismotectonics of the Garhwal Himalaya using small-to-moderate earthquakes: Implications to the local structures and free fluids. *Journal of Asian Earth Sciences*, *135*, 198-211.

49. Prasath, R. A., Paul, A., & Singh, S. (2019). Earthquakes in the Garhwal Himalaya of the Central Seismic Gap: A Study of Historical and Present Seismicity and Their Implications to the Seismotectonics. *Pure and Applied Geophysics*, *176*(11), 4661-4685.

50. Ram, V. S., Kumar, D., & Khattri, K. N. (2005). The 1986 Dharamsala earthquake of Himachal Himalaya–estimates of source parameters, average intrinsic attenuation and site amplification functions. *Journal of seismology*, *9*(4), 473-485.

51. Rastogi, B. K. (1974). Earthquake mechanisms and plate tectonics in the Himalayan region. *Tectonophysics*, *21*(1-2), 47-56.

52. Rawat, G., Arora, B. R., & Gupta, P. K. (2014). Electrical resistivity cross-section across the Garhwal Himalaya: Proxy to fluid-seismicity linkage. *Tectonophysics*, *637*, 68-79.

53. Sapkota, S. N., Bollinger, L., Klinger, Y., Tapponnier, P., Gaudemer, Y., & Tiwari, D. (2013). Primary surface ruptures of the great Himalayan earthquakes in 1934 and 1255. *Nature Geoscience*, *6*(1), 71-76.

54. Seeber, L., & Pêcher, A. (1998). Strain partitioning along the Himalayan arc and the Nanga Parbat antiform. *Geology*, *26*(9), 791-794.

55. Seeber, L., Armbruster, J. G., & Quittmeyer, R. C. (1981). Seismicity and continental subduction in the Himalayan arc. *Zagros Hindu Kush Himalaya Geodynamic Evolution*, *3*, 215-242.

56. Singh, R., Prasath, R. A., Paul, A., & Kumar, N. (2018). Earthquake swarm of Himachal Pradesh in northwest Himalaya and its seismotectonic implications. *Physics of the Earth and Planetary Interiors*, *275*, 44-55.

57. Srinagesh, D., Singh, S. K., Suresh, G., Srinivas, D., Pérez-Campos, X., & Suresh, G. (2018). A study of Guptkashi, Uttarakhand earthquake of 6 February 2017 (M w 5.3) in the Himalayan arc and implications for ground motion estimation. *Journal of Seismology*, *22*(3), 789-803.

58. Tandon, A. N., & Srivastava, H. N. (1975). Focal mechanisms of some recent Himalayan earthquakes and regional plate tectonics. *Bulletin of the Seismological Society of America*, *65*(4), 963-969.

59. Tapponnier, P., Mercier, J.L., Armijo, R., Tonglin, H. and Ji, Z., 1981. Field evidence for active normal faulting in Tibet. *Nature*, *294*(5840), pp.410-414.

60. Thakur, V. C. (1992). Geology of western Himalaya. *Physics and Chemistry of the Earth*, *19*, 1-355.

61. Thakur, V. C., & Jayangondaperumal, R. (2015). Seismogenic active fault zone between 2005 Kashmir and 1905 Kangra earthquake meizoseismal regions and earthquake hazard in eastern Kashmir seismic gap. *Current Science (00113891)*, *109*(3).

62. Vavryčuk, V., 2014. Iterative joint inversion for stress and fault orientations from focal mechanisms. *Geophysical Journal International*, *199*(1), pp.69-77.

63. Verma, M., Sutar, A. K., Bansal, B. K., Arora, B. R., & Bhat, G. M. (2015). MW 4.9 earthquake of 21 August, 2014 in Kangra region, Northwest Himalaya: Seismotectonics implications. *Journal of Asian Earth Sciences*, *109*, 29-37.

64. Verma, R. K., & Sekhar, C. C. (1986). Focal mechanism solutions and nature of plate movements in Pakistan. *Journal of geodynamics*, *5*(3-4), 331-351.

65. Wallis, D., & Searle, M. P. (2019). Spatial and Temporal Distributions of Deformation in Strike-Slip Faults: The Karakoram Fault in the India-Asia Collision Zone. In *Transform Plate Boundaries and Fracture Zones* (pp. 271-300). Elsevier.

66. Yadav, D. K., Hazarika, D., & Kumar, N. (2016). Seismicity and stress inversion study in the Kangra–Chamba region of north-west Himalaya. *Natural Hazards*, *82*(2), 1393-1409.

67. Yadav, D. K., Kumar, N., Hazarika, D., Yadav, D. N., & Wadhawan, M. (2017). Seismicity and Tectonics of Kinnaur Himalaya and adjoining region inferred from focal mechanism solutions and stress tensor inversion. *HIMALAYAN GEOLOGY*, *38*(1), 49-55.

68. Yu, Z., Zhao, D., Li, J., Huang, Z., Nishizono, Y., & Inakura, H. (2019). Stress field in the 2016 Kumamoto earthquake (M 7.3) area. *Journal of Geophysical Research: Solid Earth*, *124*(3), 2638-2652.

Author Contributions

R.A.P., B.K.B., and M.V. have conceived the research problem. R.A.P. performed data compilation and analysis. R.A.P., B.K.B., and M.V. interpreted the results. R.A.P. drafted all the figures and prepared the first draft of the manuscript. R.A.P., B.K.B., and M.V. have finalized the manuscript.

Figure Legends

Figure 1. **The western India-Eurasia Collision Zone, its Structure, Tectonics and Seismicity.** (a) Map of the study area along with the major geological structure and tectonic elements (Thakur, 1992; Thakur & Jayamgondaperumal, 2005; Wallis & Searle, 2019). (b) Epicentral locations of FM solutions used in the present study with the background seismicity from the catalog of International Seismological Center (ISC). Acronyms: AK-Almora Klippen, BBF- Balakot Bagh Fault, HFT-Himalayan Frontal Thrust, HHC-Higher Himalayan Crystallines, HS-Hazara Syntaxis, IGP-Indo Gangetic Plains, ITS-Indus Tsangpo Suture, JF-Jhelum Fault, KB-Kashmir Basin, KCR-Kaurik Chango Rift, KF-Karakoram Fault, KLRW-Kullu-Larji-Rampur Window, KW-Kishtwar Window, KXF-Karakax Fault, LGF-Longmu Gozha Fault, LH-Lesser Himalaya, MBT-Main Boundary Thrust, MCT-Main Central Thrust, MKT-Main Karakoram Thrust, MMT-Main Mantle Thrust, NPS-Nanga Parbat Syntaxis, SH-

534 Sub Himalaya, SRT-Salt Range Thrust, STD-Southern Tibetan Detachment, TH-Tethyan
535 Himalaya, TP-Tibetan Plateau.

536

537 Figure 2. **Earthquake Focal Mechanism solutions used in the present study.** Figure shows
538 the Earthquake FM solutions along with the seismotectonic zones, viz., (1) Garhwal-Kumaun
539 Himalaya, (2) Shimla, (3) Kangra-Chamba, (4) Kishtwar, (5) Hazara Syntaxis, (6) Nanga
540 Parbat Syntaxis, (7) Northwest Karakoram Fault, (8) Southeast Karakoram Fault and (9)
541 Kaurik Chango Rift. Acronyms are similar to those given in Fig. 1

542

543 Figure 3. **Major results of the study.** (a) Principle stress axes from the stress inversions
544 plotted with the respective zones. Inset-A shows the classification of stress fields (1-6) for the
545 western IECZ. Acronyms are similar to as given in Fig. 1

546

547 Figure 4. **Stress inversion plots for six stress fields categorized in the present study**. (a)
548 Principle stress and P/T axes, (b) Confidence of the stress axes, (c) Mohr circle diagram and
549 (d) Shape ratio 'R'.

550

551

552

553

Table(s)

Table 1. Results of stress inversions using earthquake focal mechanisms in the western IECZ.

ID	Zone code	Zone	Nodal planes used	Stress Orientations (Az/Pl ±Error*)			Principle FMs S1/D1/R1, S2/D2/R2†	R	μ
				Sigma 1	Sigma 2	Sigma 3			
1	1	Garhwal-Kumaun Himalaya	106	212/19 ±05.5	114/23 ±25.6	337/60 ±25.3	095/53/060, 004/25/162	0.93± 0.19	0.66
2	2	Shimla	40	208/19 ±05.7	109/25 ±19.1	331/58 ±19.1	088/52/058, 004/26/166	0.85± 0.17	0.70
3	3	Kangra-Chamba	54	248/02 ±11.1	157/12 ±17.3	346/78 ±17.2	130/25/060, 009/22/124	0.62± 0.11	1.20
4	4	Khistwar Window	66	233/10 ±03.3	324/08 ±06.8	092/78 ±06.7	155/35/103, 299/17/064	0.78± 0.06	0.85
5	5a	Hazara Syntaxis	114	212/10 ±05.7	121/06 ±05.3	360/78 ±03.5	115/45/081, 315/25/105	0.46± 0.04	0.40
6	5b	Aftershocks of 2005 Kashmir EQ	84	219/12 ±07.2	127/03 ±13.3	025/78 ±13.7	125/45/086, 315/21/098	0.60± 0.07	0.45
7	6	Nanga Parbat Syntaxis	14	083/83 ±23.5	249/07 ±29.6	339/02 ±20.7	245/60/-097, 073/57/-082	0.63± 0.28	0.50
8	7	Northwest KF	26	221/50 ±38.5	040/40 ±37.5	130/01 ±24.4	022/70/-134, 239/69/-046	0.39± 0.29	0.71
9	8	Southeast KF	26	185/17 ±09.6	067/57 ±09.6	284/28 ±06.4	039/73/029, 345/57/-175	0.65± 0.10	0.82
10	9	KCR	28	358/30 ±10.1	195/59 ±37.7	092/07 ±37.6	023/85/-031, 161/72/-155	0.53± 0.15	0.95
11	HSB	Himalayan Seismic Belt	266	210/19 ±03.1	110/27 ±15.5	331/56 ±15.5	086/51/055, 015/26/175	0.91± 0.07	0.92
12	NHSB	North of HSB (Tibet)	116	205/06 ±07.4	047/83 ±07.2	296/03 ±03.9	234/89/-007, 357/85/-176	0.40± 0.06	0.64
13	All dataset	Whole region	490	214/13 ±02.0	121/11 ±13.3	353/73 ±13.3	108/41/073, 342/17/132	0.87± 0.03	0.77
14	1+2	Garhwal-Kumaun-Shimla	146	210/19 ±03.0	110/27 ±20.0	331/56 ±20.1	086/51/055, 015/27/176	0.90± 0.08	0.91
15	3+4	Kangra-Chamba-Khistwar	120	237/08 ±03.5	146/04 ±07.8	032/81 ±07.0	140/32/083, 339/16/104	0.72± 0.03	0.94
16	8+9	Southeast-KF and KCR	54	180/06 ±13.9	057/79 ±15.8	271/09 ±9.04	030/85/010, 332/79/-179	0.52± 0.09	0.64

*Az-Azimuth, Pl-Plunge, S1/S2-Strike 1 and 2, D1/D2-Dip 1 and 2, R1/R2-Rake 1 and 2, R-Shape ratio and μ-Friction Coefficient. *Errors are common for both Azimuth and Plunge values.*

Figure 1.

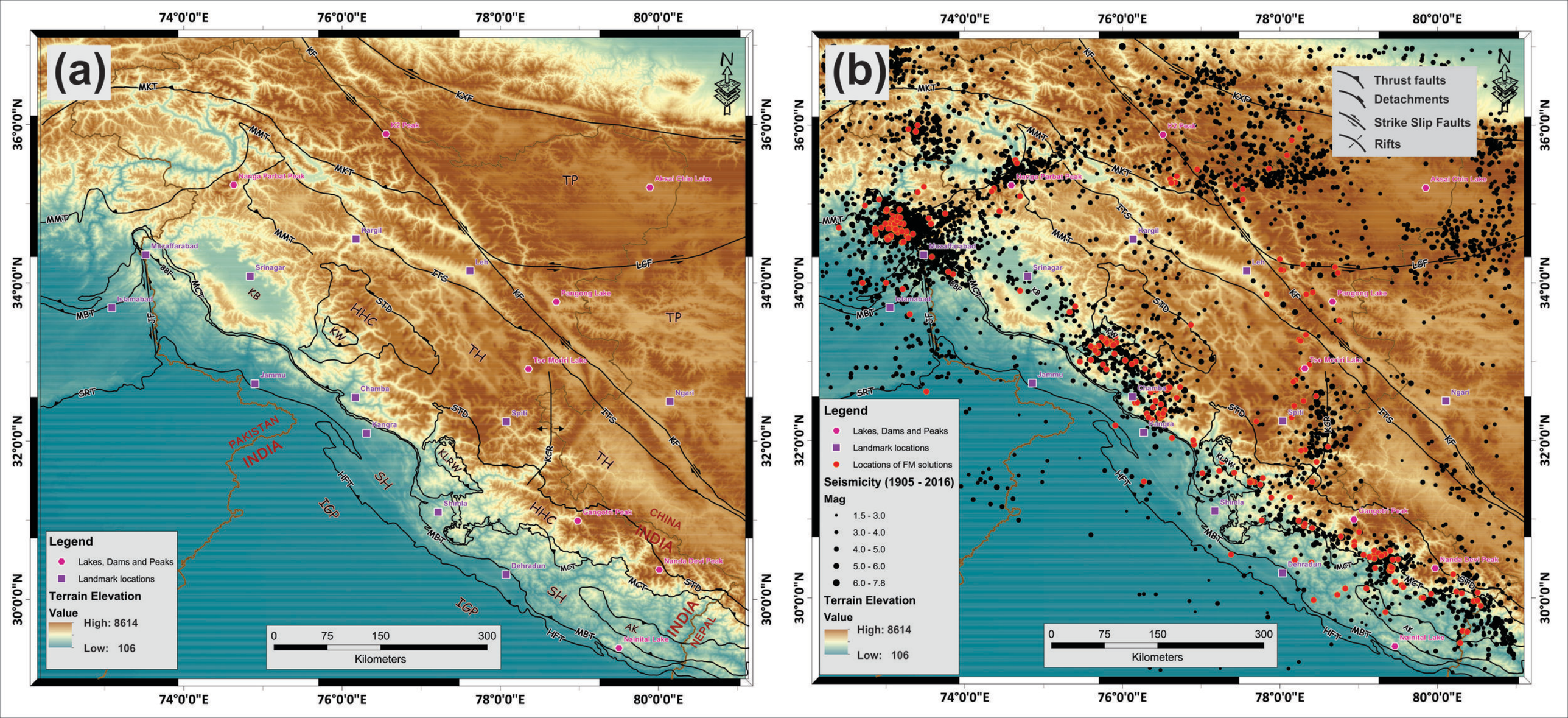
(a)
(b)
74°0'0"E
76°0'0"E
78°0'0"E
80°0'0"E
36°0'0"N
34°0'0"N
32°0'0"N
30°0'0"N
N
MKT
KF
KXF
MMT
MBT
MCT
STFD
ITFS
LGF
HFT
SRT
JF
BBF
KLRW
KCR
K2 Peak
Nanga Parbat Peak
Aksai Chin Lake
Kargil
Muzaffarabad
Srinagar
Leh
Pangong Lake
Islamabad
Jammu
Chamba
Ngari
Tso Moriri Lake
Spiti
Kangra
Shimla
Gangotri Peak
Nanda Devi Peak
Dehradun
Nainital Lake
KB
KW
HHC
TH
TP
SH
IGP
PAKISTAN
INDIA
CHINA
NEPAL
AK
Thrust faults
Detachments
Strike Slip Faults
Rifts
Legend
Lakes, Dams and Peaks
Landmark locations
Locations of FM solutions
Seismicity (1905 - 2016)
Mag
1.5 - 3.0
3.0 - 4.0
4.0 - 5.0
5.0 - 6.0
6.0 - 7.8
Terrain Elevation
Value
High: 8614
Low: 106
0
75
150
300
Kilometers

Figure 2.

74°0'0"E
76°0'0"E
78°0'0"E
80°0'0"E
36°0'0"N
34°0'0"N
32°0'0"N
30°0'0"N
N
MKT
KF
KXF
MMT
Nanga Parbat Peak
K2 Peak
Aksai Chin Lake
Zone 6
Zone 7
Kargil
Muzaffarabad
Srinagar
Leh
LGF
I-TSZ
BBF
KB
Islamabad
MBT
MCT
STD
Pangong Lake
KF
Zone 5
Zone 8
KW
Tso Moriri Lake
Jammu
SRT
Zone 4
Chamba
Ngari
Spiti
KCR
Kangra
HFT
KLRW
Zone 9
Zone 3
Shimla
Gangotri Peak
Zone 2
Dehradun
Nanda Devi Peak
AK
Nainital Lake
Zone 1
Legend
Lakes, Dams and Peaks
Landmark locations
Locations of FM solutions
Terrain Elevation
Value
High: 8614
Low: 106
Size Chart for FM Solutions
Mag 7.0- 8.0
Mag 6.0- 7.0
Mag 5.0- 6.0
Mag 4.0- 5.0
Mag 3.0- 4.0
0
75
150
300
Kilometers

Figure 3.

Legend

- Lakes, Dams and Peaks
- Landmark locations

Terrain Elevation Value

High: 8614

Low: 106

Horizontal Stresses

Sigma 1

Sigma 2

Sigma 3

Vertical Stresses

- Sigma 1
- Sigma 2
- Sigma 3

74°0'0"E 76°0'0"E 78°0'0"E 80°0'0"E

36°0'0"N 34°0'0"N 32°0'0"N 30°0'0"N

N

MKT KF KXF MMT LGF ITS STD MCT MBT BBF JF SRT HFT KCR KLRW IGP SH TH TP KB KW HHC AK

K2 Peak Nanga Parbat Peak Aksai Chin Lake Kargil Leh Srinagar Muzaffarabad Islamabad Pangong Lake Tso Moriri Lake Jammu Chamba Kangra Spiti Ngari Shimla Gangotri Peak Dehradun Nanda Devi Peak Nainital Lake

Zone 1 Zone 2 Zone 3 Zone 4 Zone 5 Zone 6 Zone 7 Zone 8 Zone 9

PAKISTAN INDIA CHINA NEPAL

0 75 150 Kilometers

INSET A

0 75 150 300 Kilometers

HSB | Western Tibet | Gahwal-Kumaun Shimla | Kanga-Chamba Kishtwar | Southeast KF KCR | All dataset

Figure 4.

Stress Field I

(a)

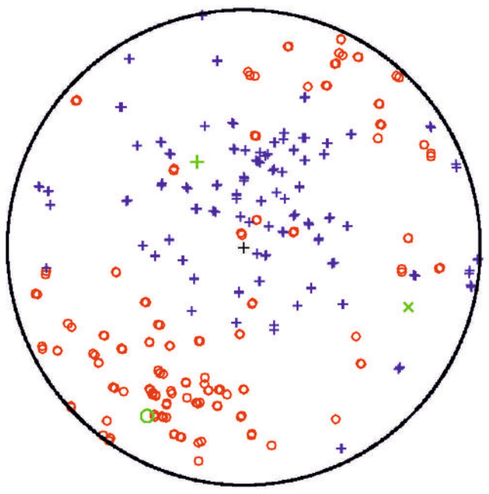

(b)

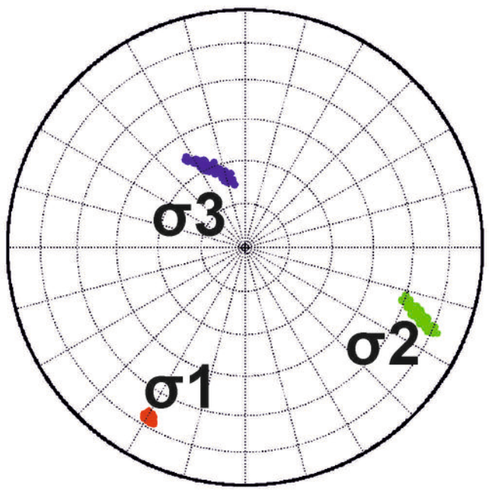

(c)

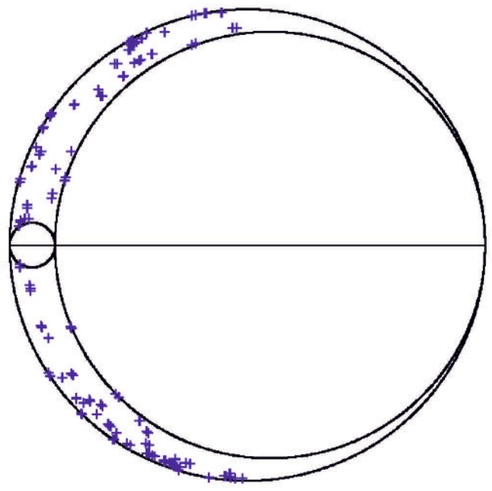

(d)

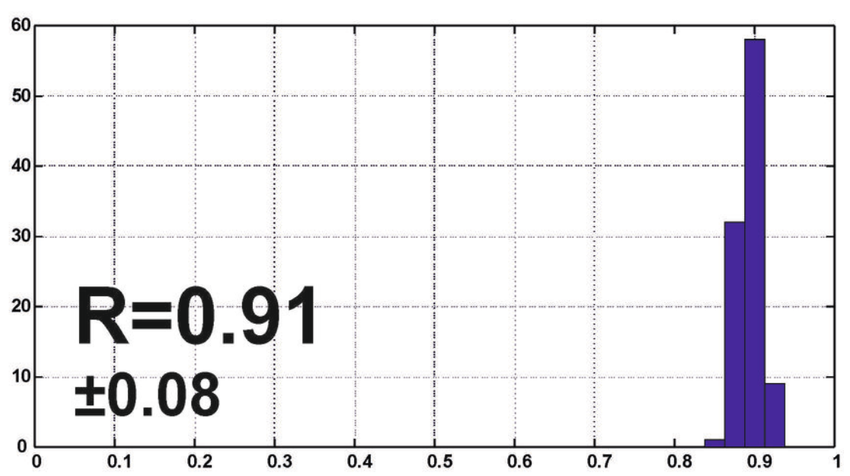

Stress Field II

(a)

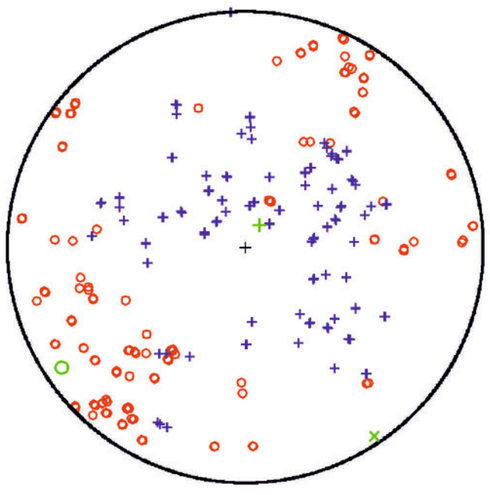

(b)

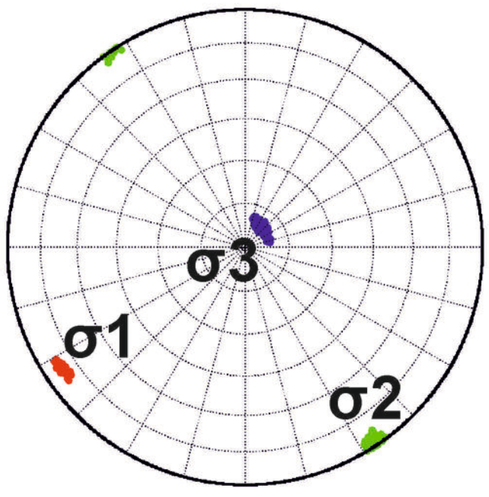

(c)

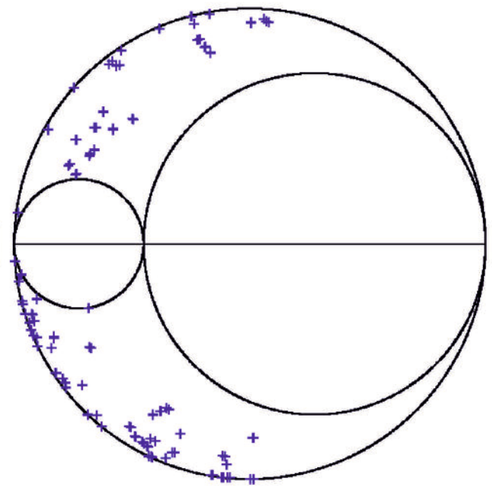

(d)

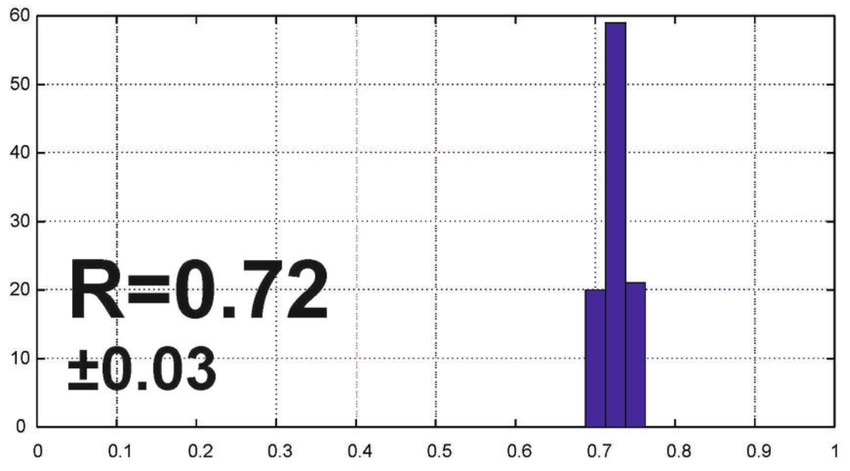

Stress Field III

(a)

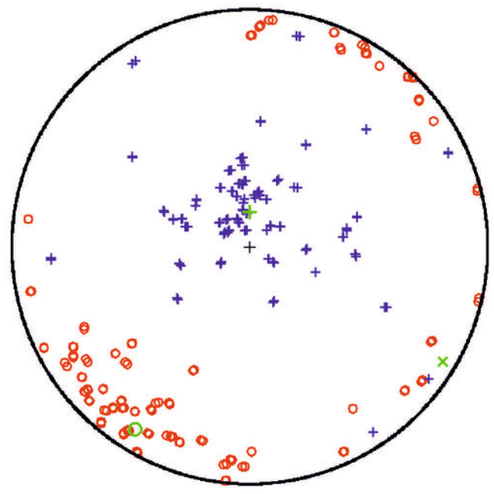

(b)

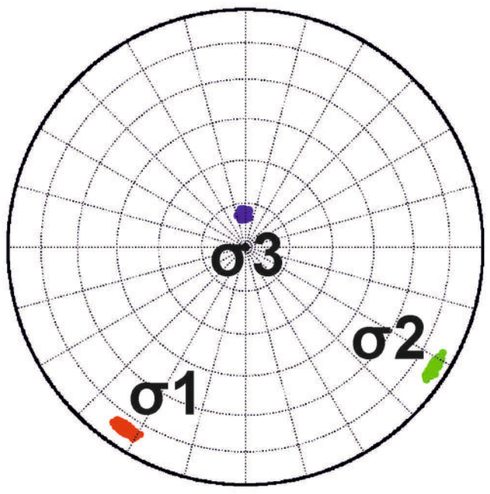

(c)

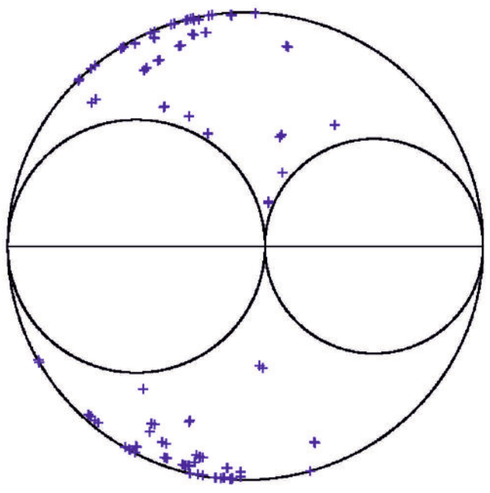

(d)

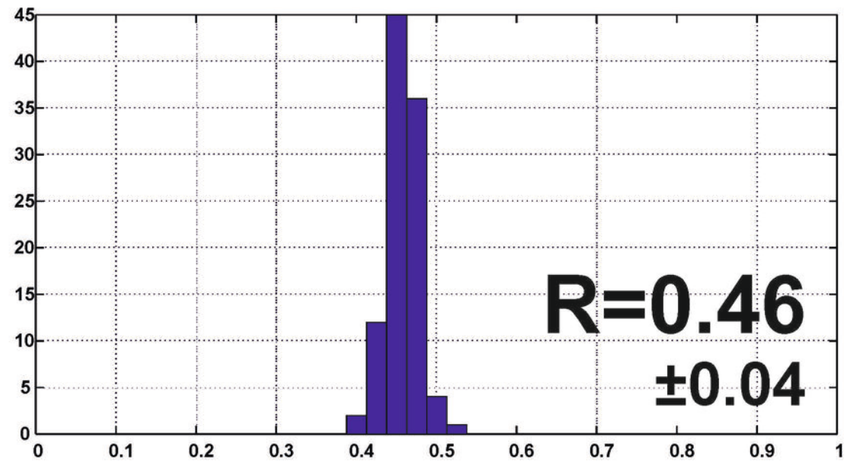

Stress Field IV

(a)

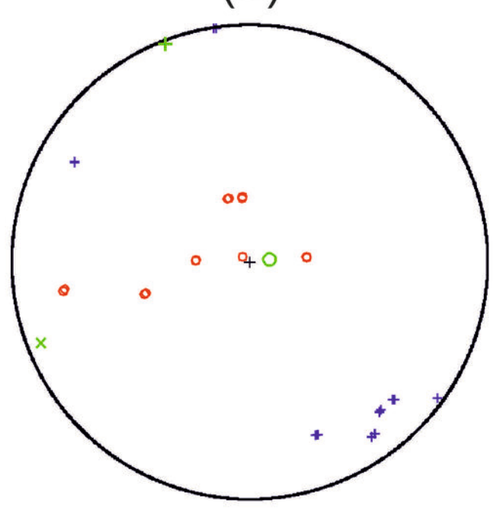

(b)

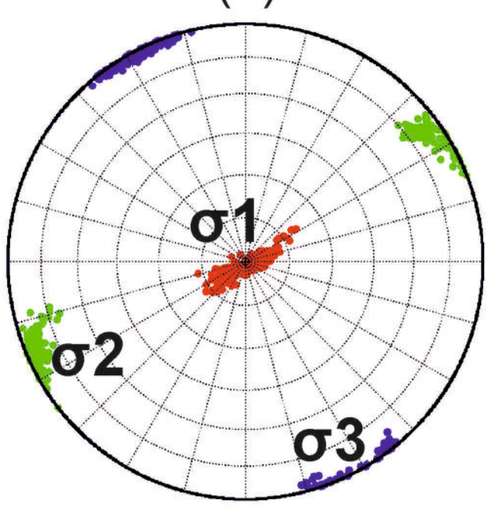

(c)

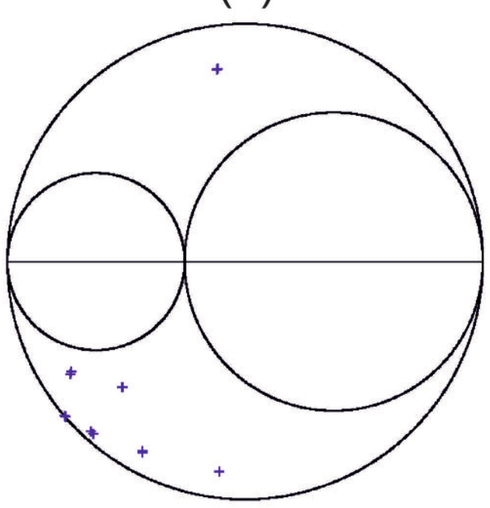

(d)

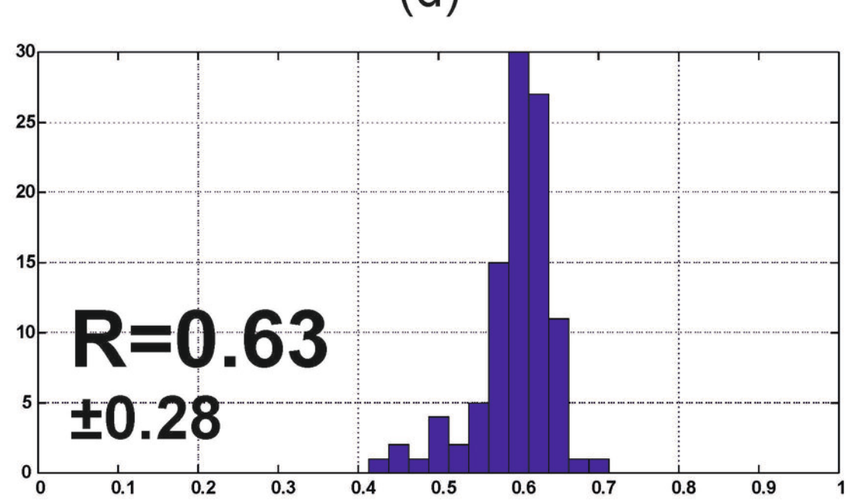

Stress Field V

(a)

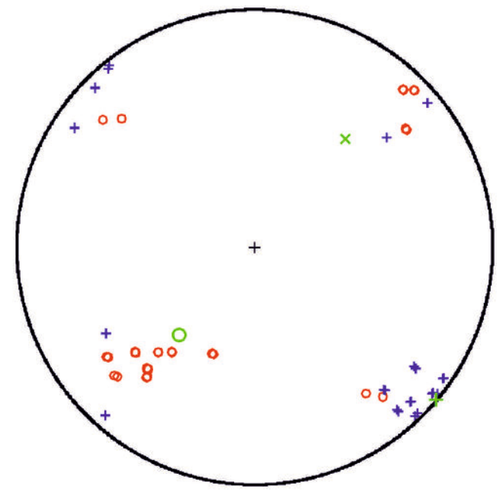

(b)

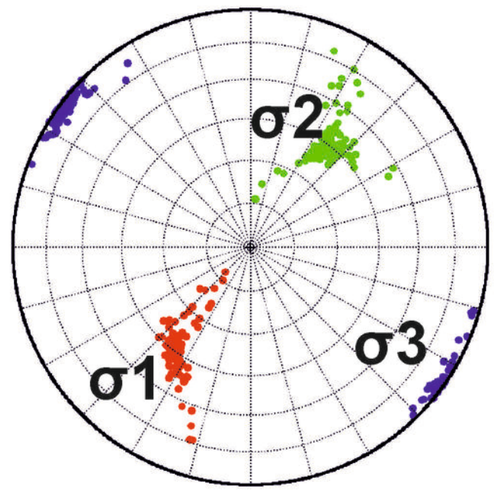

(c)

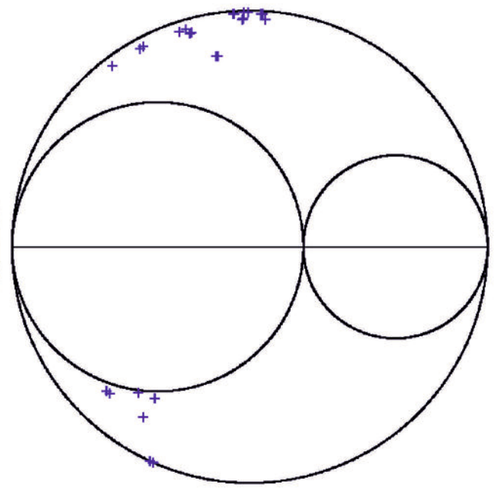

(d)

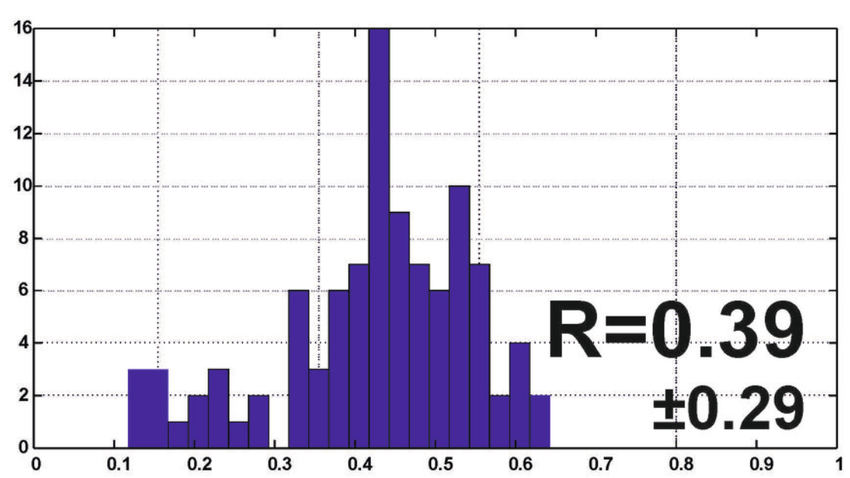

Stress Field VI

(a)

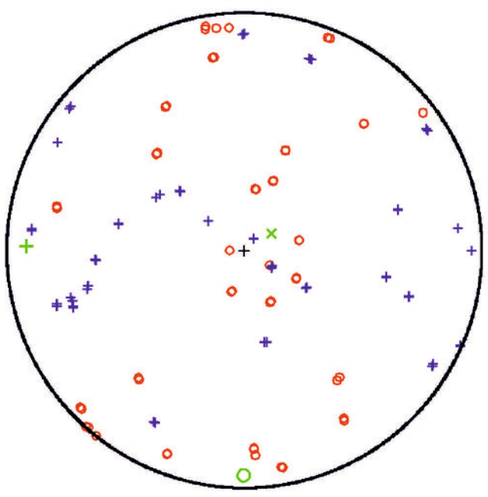

(b)

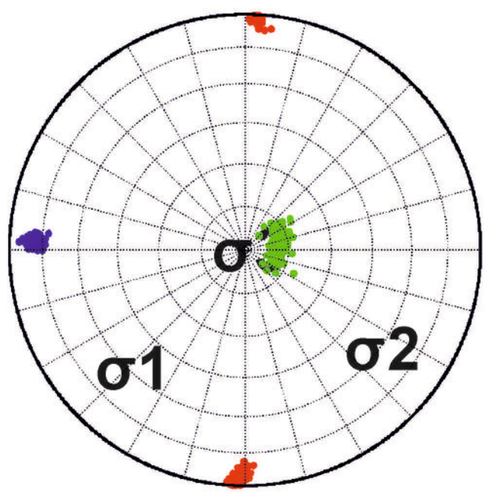

(c)

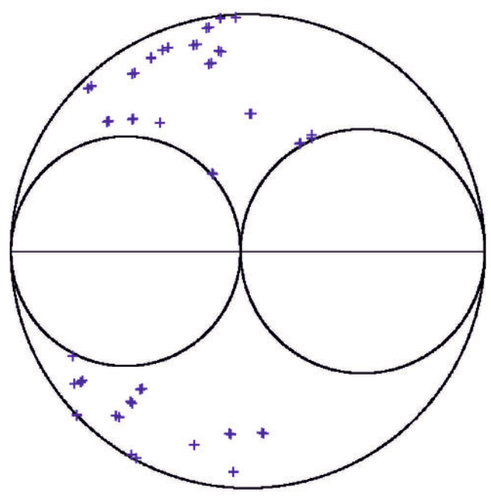

(d)